LASER & PHOTONICS REVIEWS
www.lpr-journal.org

Multi-Functional Optical Neural Network in a Disordered Medium

*Hengzhe Yan, Yuncong Sun, Yijia Yu, Ruixin Ma, Xianfeng Chen, Yuping Chen, and Wenjie Wan**

Optical neural networks leverage the speed and parallelism of light to process information. However, many prior works are highly resource-intensive and lack multi-task ability. Here, a multi-functional optical neural network based on wavefront shaping in a nonlinear disordered media is proposed. The setup can serve as either a linear or nonlinear neural network, where the input field is modulated by a spatial light modulator, and all the modulated modes are interconnected via random scattering in the disordered media. An adaptive training pipeline is built based on the separable natural evolutionary strategies. This versatile and low-cost system can perform a range of computational imaging tasks, including beam mode decomposition and image reconstruction through diffusers, without necessitating wavefront sensing or transmission matrix measurement. Additionally, its applicability to classical machine learning tasks, specifically image classification is demonstrated. These results collectively indicate that this optical neural network presents a promising platform for high-speed computational imaging and machine learning with potential implications for various fields.

1. Introduction

The soaring demand for computational resources in artificial intelligence has spurred the development of innovative computing platforms. Optical neural networks (ONNs), renowned for their exceptional processing speed and parallel capabilities, have emerged as promising candidates for diverse applications,[1–3] such as computer vision,[4–9] computational imaging,[10–13] optical communication[14,15] and time-series prediction.[16,17] In an ONN, the optical interconnect is crucial to connecting the modulated optical modes and achieving parallel data processing. Up to now, various optical interconnect architectures have been implemented, including Mach-Zehnder interferometers,[16,18] Dammann grating,[17] microlens array,[13] Fourier lens,[18] free space diffraction,[4,9] and fiber multiplexer.[19] Among them, the diffraction-based ONN can reach a much larger scale and thus perform more complex tasks by modulating light spatial modes with multiple diffraction surfaces[9] or spatial light modulators (SLMs).[4] Additionally, since ONNs operate directly on the wavefront, they are well-suited for advanced imaging problems such as scattering imaging[10–12] and modal decompositions.[20–22] Those problems would otherwise be complex and time-consuming using traditional solutions that require wavefront measurements.[23] However, the diffraction surfaces are usually fixed and can only perform the pre-designed tasks. In recent years, multi-functional ONNs have also been demonstrated based on pluggable diffraction surfaces,[24,25] while still requiring mechanical operations. Meanwhile, ONNs based on multiple SLMs are proposed, which can be trained adaptively for various tasks.[4] However, the multiple-SLM configuration makes the system bulky and expensive.

Alternatively, a disordered medium can efficiently interconnect the incident wave through multiple scattering and such connections are independent of the spatial structures of the input modes.[26] This interconnection replaces the free-space propagation between the multiple SLMs in usual diffraction ONNs and hence only one SLM is required. The disordered sample is easy to fabricate and does not require complex alignment and calibration. Despite the seemingly randomness, the light scattering process is deterministic for a stationary disordered medium. Such a disordered system can be fully described by a linear transmission matrix (TM)[27,28] and it is still possible to control the light field behind it with wavefront shaping. The nearly infinite number of scattering modes provides a possibility to build a multi-functional platform reconfigurable for various tasks.

Previously, a universal linear operator has been proposed based on a disordered medium and an SLM,[29] in which by measuring the transmission matrix and optimizing the SLM pattern, the system can serve as a universal operator. Several different linear operators are realized in their setup. Due to issues such as mechanical instability in the transmission matrix measurement, the operator dimension is restricted quite small (16

H. Yan, Y. Sun, Y. Yu, R. Ma, W. Wan
State Key Laboratory of Photonics and Communications
University of Michigan-Shanghai Jiao Tong University Joint Institute
Shanghai Jiao Tong University
Shanghai 200240, China
E-mail: wenjie.wan@sjtu.edu.cn
X. Chen, Y. Chen, W. Wan
Department of Physics and Astronomy
Shanghai Jiao Tong University
Shanghai200240, China

The ORCID identification number(s) for the author(s) of this article can be found under https://doi.org/10.1002/lpor.202501407

DOI: 10.1002/lpor.202501407

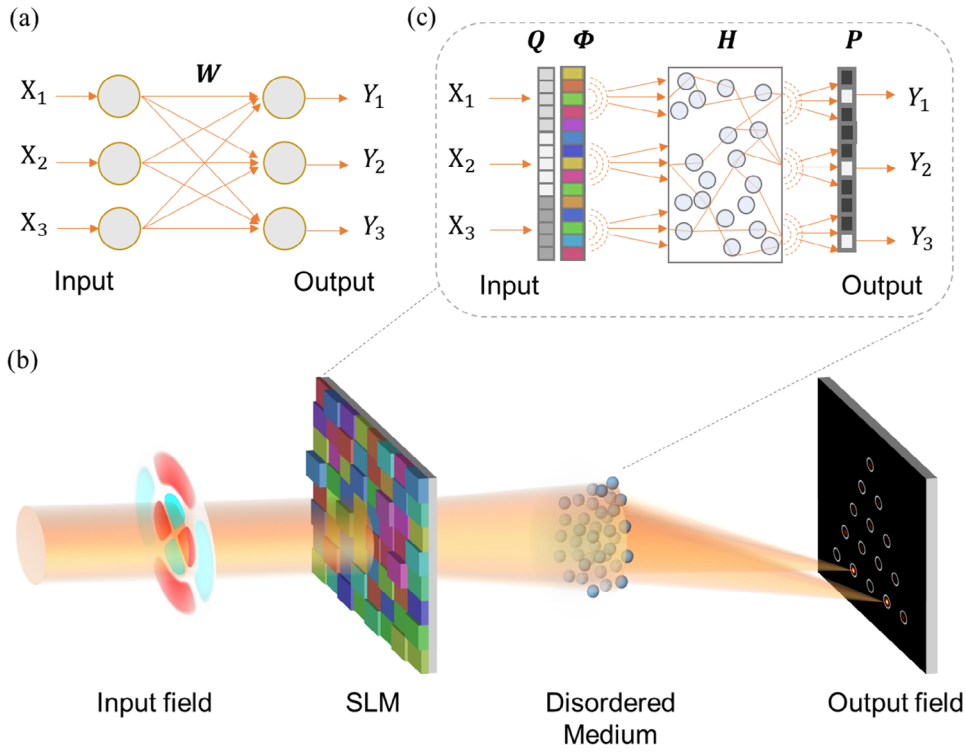

Figure 1. Schematic diagram of the optical neural network based on disordered medium. a) The architecture of a single-layer fully connected neural network. b) The setup of an optical neural network and an example of its function for LG modal decomposition. An input LG beam is modulated by SLM and scattered in the disordered medium so that two focal spots form in the output plane to decompose the LG mode. c) The architecture of our optical neural network is analogs to the conventional neural network. The input field is modulated by the SLM and then all modulated modes are connected by the disordered medium after multiple scattering.

× 16). Moreover, the random nature of the disordered medium has also been utilized for accelerators,[30] where the disordered medium works together with a digital neural network and helps improve performance. Meanwhile, the disordered medium is an excellent platform for nonlinear optical processes such as second harmonic generation (SHG) thanks to the random quasi-phase-matching. [31,32] Compared with other types of optical nonlinearity such as fluorescence and electrical-induced transparency,[2,3] the SHG is instantaneous and suitable for high-speed computing. Recently, nonlinear disordered mediums have been utilized as optical encoders to extract image features in image classification,[33] which indicated that nonlinearity can significantly improve performance. However, it still requires digital regressions to decode the random speckle patterns on the camera. To our knowledge, no prior work has employed the architecture of nonlinear disordered medium and SLM as an independent optical neural network.

In this work, we experimentally demonstrated a multifunctional ONN in a disordered medium. An adaptive training process is developed for constructing large-scale optical operators based on the Separable Natural Evolutionary Strategies (SNES) algorithm. We leverage the phase-sensitive property of the disordered medium and demonstrated that the ONN can perform real-time computation imaging tasks including beam modal decomposition and scattering imaging, which would otherwise require interferometers or other complicated devices for wavefront measurement. The inferring processes of the ONN are performed all optically and thus finished instantaneously. Moreover, the ONN can perform basic machine learning tasks such as hand-written digit classification. Finally, based on the SHG process in a disordered medium, we build a nonlinear ONN for LG modal classification. All those results indicate that the proposed ONN is a promising platform for high-speed computational imaging and machine learning, paving the way in various fields such as optical communications and autonomous driving.

2. Principle

The typical architecture of a single-layer neural network is shown in **Figure 1a**, where all the input nodes X are inter-connected via the weighted coefficient matrix W to determine the output Y. Namely, $Y = WX$. The matrix W is adaptively adjusted based on the output's feedback to obtain the optimal one for the current task. The node connection is realized with various optical interconnect methods as introduced in Section 1. In our ONN, the disordered medium is used for the interconnection. First, the input light field is spatially modulated by the phase mask displayed on the SLM (Figure 1b). Each spatial mode diffracts slightly as in previous diffraction neural networks[9] and is then scattered by the disordered medium. The disordered medium connects all the modulated spatial modes together via multiple scattering (Figure 1c). The output speckle pattern after scattering is finally captured by an image sensor or detector array. Supposing the input is represented by an $N \times 1$ vector, the output is $M \times 1$, the

SLM is divided into L segments, and the optical interconnection can be described by:

$$W = PH\Phi Q \tag{1}$$

where W is the target operator of size $M \times N$, Q is a $L \times N$ binary matrix representing the up-sampling of the field on the SLM plane, Φ is a $L \times L$ complex diagonal matrix representing the modulation on the SLM segments, matrix H is $L \times L$ transmission matrix that describes the light propagation and scattering, P is the $M \times L$ downsampling matrix realized by selecting pixel positions in the image sensor. It is assumed that the scattering is sufficiently strong so that the transmission matrix H is random and all its elements are independent random variables in circular Gaussian distribution.[27] Under this assumption, it is proven (Section S4, Supporting Information) that for a given operator W in size $M \times N$, Equation (1) has solutions for the SLM modulation matrix Φ if the SLM segments number L satisfies $L > MN$. Therefore, this architecture can work analogously to a digital single-layer linear neural network and the minimum SLM segment number is determined by the corresponding digital operator's size. For example, for a classical linear image classifier trained for the MNIST dataset, the operator size is 784×10 and it only requires 7840 SLM segments to ensure that Equation (1) has a solution. In principle, current SLMs usually possess millions of pixels and can be divided into sufficient segments to achieve perform this task. However, since the transmission matrix is hard for accurate measurement, this architecture was only demonstrated for small-size operators previously.[29] Therefore, instead of measuring the transmission matrix, we develop an adaptive training process based on the SNES algorithm[34,35] for adaptively training the SLM pattern.

Considering an optical classifier to train, there are M different DMD patterns and M corresponding pixels selected in the camera sensor. The SLM pattern is divided into L segments to be adaptively trained based on the feedback from the camera. For an ideal SLM pattern, when displaying one of the DMD patterns, the light should be perfectly focused on the correct spot corresponding to that pattern. Therefore, to quantitatively evaluate the performance of the SLM patterns, the objective function is defined to be the cross-entropy function:

$$f(z) = \sum_{i=1}^{M} \sum_{j=1}^{M} Y_{ij} \log I_{ij}(z) \tag{2}$$

where z is the vectorized SLM pattern with size $1 \times L$, I_{ij} is the light intensity at the spot "i" when displaying the DMD pattern indexed "j", $Y_{ij} = 1$ for $i = j$ and $Y_{ij} = 0$ for $i \neq j$. Since $I_{ij}(z)$ is dependent on the unknown transmission matrix of the scattering sample, it is hard to get the gradient information of this function and use the conventional gradient descent algorithm for training. Therefore, we train the SLM pattern based on SNES, which evaluates the natural gradient by multiple sampled results. Concretely, during each iteration step, K different SLM patterns denoted as z_k are randomly generated obeying the Gaussian distribution with expectation μ and standard deviation σ. The objective function for the distribution parameter (μ, σ) is also evaluated by the K samples: $J(\mu, \sigma) = \sum_{k=1}^{K} f(z_k)$. For each iteration step, the parameters are adjusted toward the natural gradient direction of the objective function:

$$\mu' = \mu + \eta_\mu \nabla_\mu J, \sigma' = \sigma \exp\left(\frac{\eta_\sigma}{2} \nabla_\sigma J\right) \tag{3}$$

where η_μ, η_σ are the learning rates, $\nabla_\mu J$ and $\nabla_\sigma J$ are the evaluated natural gradients.[34] After that, the new set of SLM patterns is generated according to Gaussian distribution with the updated parameters. The above iteration repeats until the time limit.

The experiment setup is built based on the principle in Figure 1, and more details are described in Section S1 (Supporting Information). The disordered sample is fabricated by depositing $LiNbO_3$ powders on a glass substrate via electro-phoresis. The scattering mean free path is $\approx 1.8\ \mu m$ as measured by a coherent backscattering experiment (Section S5, Supporting Information). The thickness is $\approx 100 \mu$m by measuring the power transmittance, which indicates that the ballistic photons can be neglected and the sample can be modeled as a random transmission matrix.[27] The meta parameters in the training are: sample number $K = 50$, learning rates $\eta_\mu = 1$ and $\eta_\sigma = 0.04$. As a test, a parallel light beam is focused through the disordered medium via adaptive training in SNES (Section S2, Supporting Information) under the given parameters, and achieves an enhancement factor of up to 2300, which indicates that $\approx$3000 segments or spatial modes[27] can be modulated independently for our setup. By numerical simulations, we find that such a mode number is sufficiently large for various tasks (Section S3, Supporting Information).

3. Experimental Section

First of all, we demonstrate a real-time beam modal decomposition by taking advantage of the phase-sensitive property of the disordered medium.[36] The modal decomposition is highly needed in multimode fiber communication and has been previously realized in different systems.[20–22] We test our setup in this task as a primary demonstration. Here, the LG modes are first generated with binary holograms displayed on DMD based on the superpixel method.[37,38] The modulated light beam composed of LG basis is the input of our ONN (**Figure 2**a). The light beam is modulated by the phase mask on the SLM and scattered by the disordered sample. The output pattern is then captured by the camera, where 15 sampling positions are pre-selected and each one corresponds with an LG mode. The light intensity distribution at those sampling positions identifies the mode spectrum of the input light beam. Originally, a random phase mask was displayed on the SLM and captured images are also random speckles. Then, the speckle pattern for all LG modes is captured in sequence periodically. The cross-entropy function (Equation 2) is calculated with the light intensity at those sampling spots. The phase mask on the SLM is then adaptively adjusted according to Equation (3). After such adaptive training, each one of the LG modes is focused on its target pixel in the output plane. Then, for an arbitrary input mode, by comparing the light intensity distribution at all the sampling spots, the mode is identified, as in (Figure 2a) where the mode should be identified as (1,0) with azimuthal order $l = 1$ and radial order $m = 0$. The field profile of all the 15 modes are shown in Figure 2b. The output speckles for two different modes are shown in Figure 2c, indicating that both two modes are identified correctly. Note that the speckle outside the circular sampling regions is out of our interest and is digitally filtered away only for better illustration. By recording light intensity distributions in sampling spots for all the 15 modes, a transfer matrix between input modes and output spots is obtained in Figure 2d, given a Signal-Noise-Ratio SNR $\approx$ 33. Here, the SNR is defined as the ratio between the average of the transfer matrix's diagonal elements and off-diagonal elements. Furthermore, for the incident

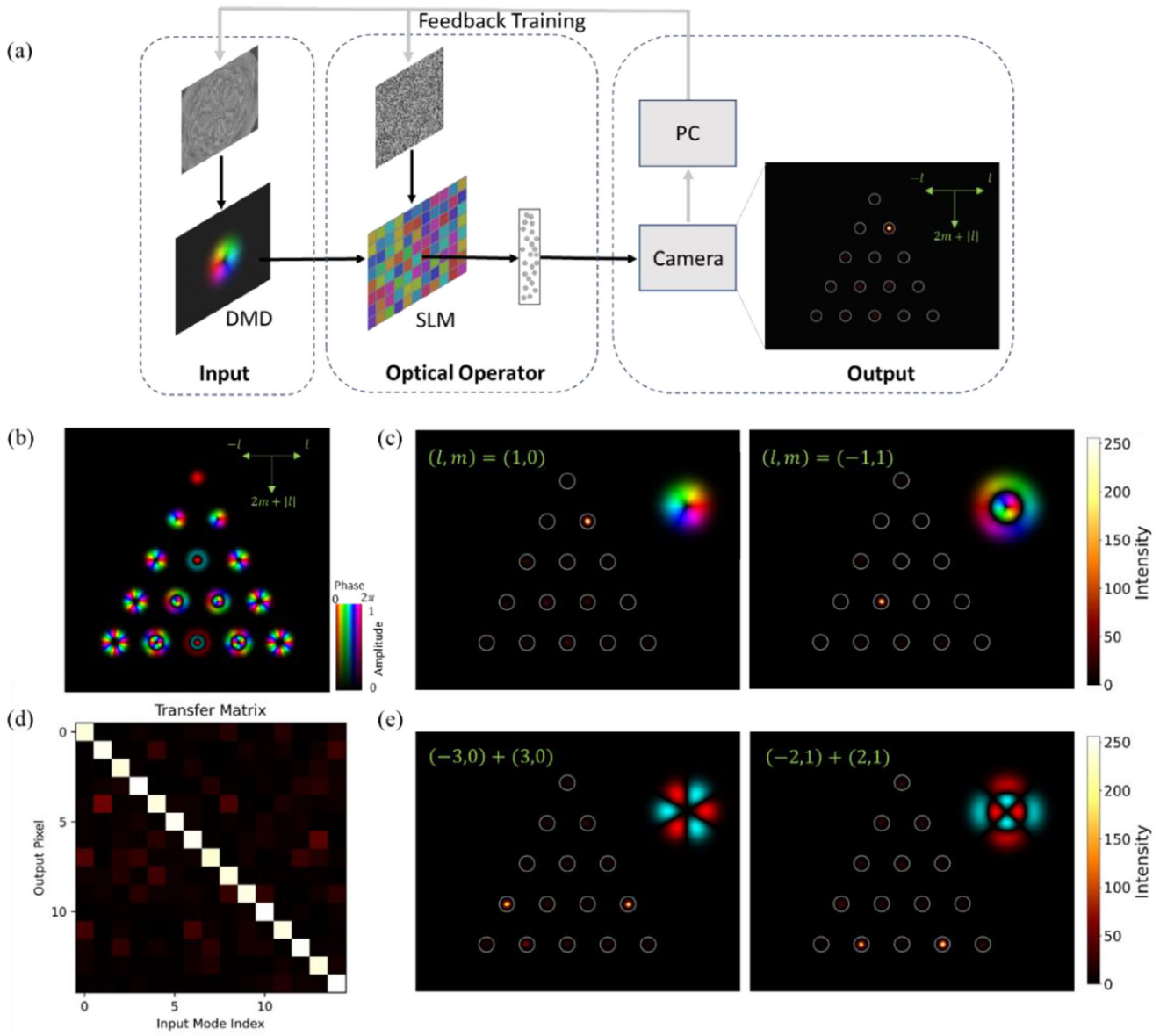

Figure 2. LG mode classification and decomposition through ONN. a) Experiment schematic diagram: a laser beam is modulated by the binary hologram displayed on DMD to be the LG (1,0) mode. The mode is as the input of the optical neural network and then modulated by the SLM and scattered by the disordered medium. After that, the light beam is focused on the sampling position corresponding with mode (1,0). b) The field profile for all the 15 LG modes. c) Classification results for input mode (1,0) and (−1,1). d) Transfer matrix between input mode and output spot. e) Modal decomposition for two different input-composed modes.

light beam composed of multiple modes, multiple focused spots emerge in the output plane. Thus, the system can also realize modal decomposition (Figure 2e). The fields of two LG modes are summed to form a composed one (Figure 2e). The composed field is projected by the DMD with the superpixel method. In the ONN, bright spots emerge at the two corresponding positions simultaneously and hence the field is decomposed. Meanwhile, the theoretical analysis (Section S3, Supporting Information) concludes an approximated scaling law: $SNR \approx L/M$, which matches the simulation results and indicates that the SNR can be improved in a linear trend by controlling more SLM segments.

As a kind of neural network, our setup can also perform image classification. We demonstrate it with hand-written digit classification based on a subset of the MNIST datasets. Similar to beam modes classification, the phase pattern on the SLM is also adaptively optimized so that when the DMD displays different digits, the scattered light beam is focused on different spots (**Figure 3a**). Four examples of classification results are shown in Figure 3c. After projecting 400 test images and capturing the output speckle, we calculated the classification confusion matrix Figure 3d and the classification accuracy is ≈83%. Our simulation (Section S4, Supporting Information) indicates that the accuracy can be further improved and reach 90% with more controllable segment numbers, approaching the performance of digital linear neural networks.[9] For the experiment, the controllable segment number is limited by mechanical instability,[27] which could be improved in the future.

Next, we use the setup for image transmission through a diffuser. The transmission matrix method is a universal technique for imaging through

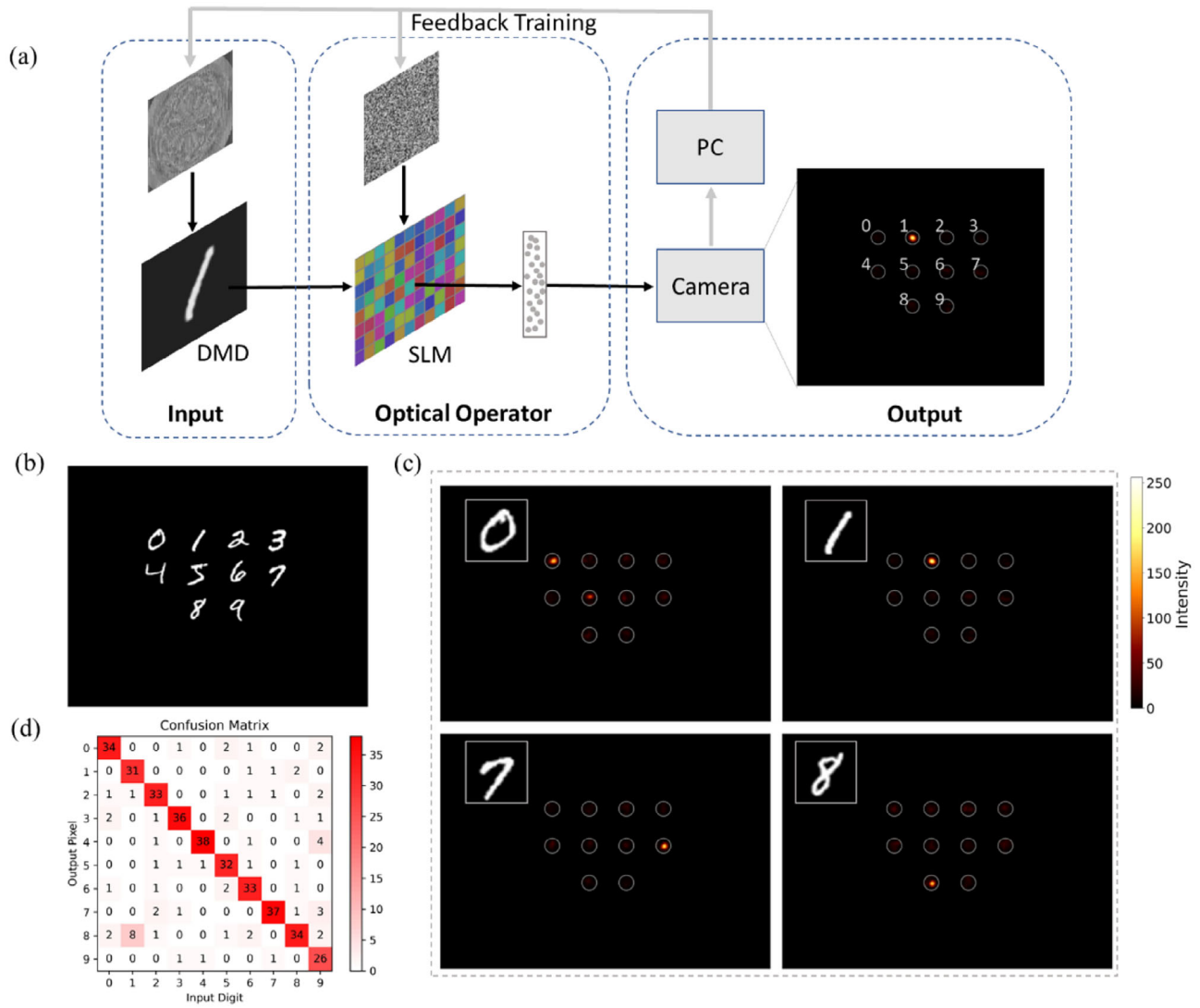

Figure 3. Hand-written digits classification. a) Experiment schematic diagram: A laser beam illuminates the DMD and an image of digits "1" is projected. With the optical operator composed of an SLM and disordered medium, the light beam is focused onto the corresponding sampling spot. b) Example of test digits for our ONN c) Four examples of successful classification results of the digits. d) The confusion matrix.

strongly disordered medium,[23] since it does not rely on ballistic photons or memory effects compared with other methods.[39–41] However, to obtain the transmission matrix, one needs to implement interferometer measurements, which is very complicated and time-consuming.[28] The image reconstruction also requires phase measurement of the scattered field and matrix inversion,[23] severely limiting the imaging frame rate. In our setup, to avoid those issues, the transmission matrix is not measured directly. Instead, we train the ONN so that it realizes the transmission matrix inversion optically.

As in **Figure 4a**, an image of the alphabet is projected by the DMD and then scrambled to random speckle patterns by a diffuser. The scattered speckle is then modulated by the SLM and scattered again by the disordered sample as before. For the output plane, we also select a grid of pixels to form the reconstructed image. Practically, we deal with low-resolution images consisting of 5 × 7 pixels. With an optimized SLM phase pattern, the original alphabet image is optically reconstructed in the output plane. For the optimization, the DMD displays 5 × 7 "one-hot" images where only one pixel is bright in sequence, and the SLM pattern is trained adaptively with the SNES as before. When turning on different pixels, the light is scattered and forms totally different speckle patterns after the first diffuser (Figure 4b,c, inset). However, after the trained ONN, the scattered light beams are focused again to their corresponding target spot in the output plane (Figure 4b,c). By capturing the output images for all 35 input pixels, we measured the transfer matrix between input and output pixels (Figure 4d), showing the SNR is ≈40. Then, we turn on two input pixels and the corresponding two output pixels also get bright (Figure 4e). In this way, it can realize the optical reconstruction of scattered images, as demonstrated for the four alphabet images in Figure 4f. Here, to eliminate the spatial coherence at the input pixels that is absent in most imaging cases with incoherent light illumination, the input image is displayed in a time-division multiplexing way where different pixels are modulated individually in sequence.

Since our optical neural network does not involve wavefront measurement or complex data processing as in previous works, it can reconstruct the image behind diffusers in real-time. Moreover, the ONN is trained based on the one-hot images for all the pixels, instead of datasets of some particular types of images such as MNIST in previous works.[12,42] Therefore, the trained ONN is adaptable for images with 5 × 7 pixels in arbitrary

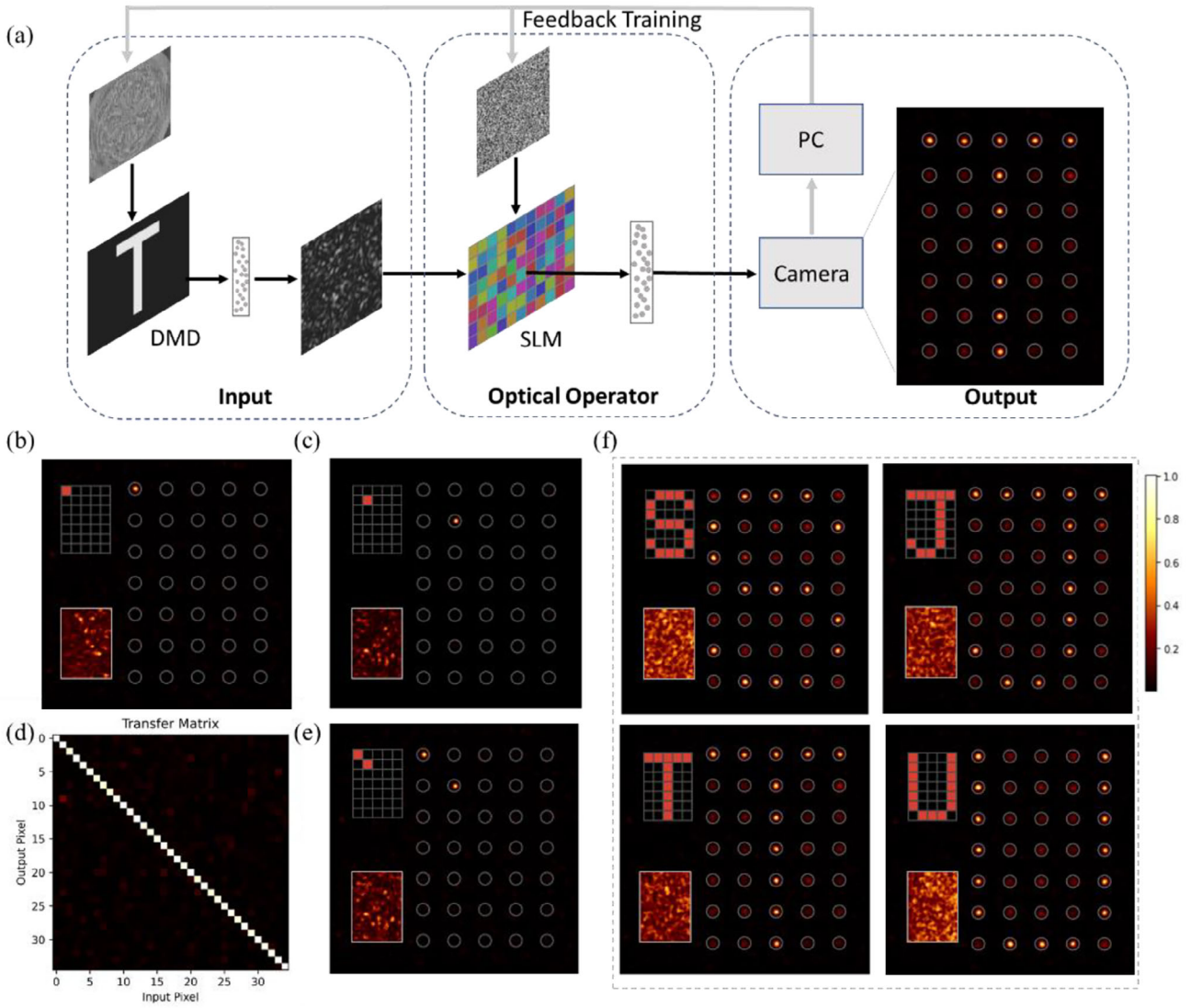

Figure 4. Real-time image transmission through diffuser. a) Experiment schematic diagram: the original image of character "T" is projected by the DMD and scrambled to random speckles by the diffuser. The random speckle is the system input. With an optical operator composed of an SLM and disordered medium, the original image is optically reconstructed in the output plane. b,c) Output for two different input pixels. In the output plane, the light is focused onto different pixels for the two cases. d) The transfer matrix between input and output pixels. e) Output image when both the two input pixels in (b,c) are turned on. f) image reconstruction results for images of four characters "SJTU".

structures. As a demonstration, we project a comic video (Supplementary) with the DMD. After adaptively training the SLM phase pattern as before, each one of the frames is optically reconstructed at the output plane without any delay. Several subsequent frames with a duration of 10 ms are shown in **Figure 5**, indicating that the video is faithfully reconstructed.

Though we mainly study linear ONN in this work, the setup can also serve as a nonlinear ONN based on the second harmonic generation (SHG) of Lithium Niobite powders in the disordered medium. The experiment setup is basically the same as the linear one. The major difference is that the light source is replaced by a pulsed laser in 1064 nm and the harmonic speckle pattern in 532 nm is recorded. Based on the scalar wave approximation,[33] such a nonlinear process can be roughly modeled in a similar form to the linear model by: $Y = PH_2|H_1\Phi QX|^2$, where Q is the up-sampling function, Φ is the SLM's modulation matrix, H_1 is the transmission matrix of the disordered medium for fundamental light, H_2 is the transmission matrix for harmonic light, the modular square operation comes from the SHG process, and P is the downsampling matrix. Similar to the linear networks, the nonlinear network is controllable by modulating the SLM pattern, and hence can be trained with the same pipeline as that in Figure 2a. As a demonstration, the nonlinear network is utilized for the modal classification of the 15 modes (**Figure 6a**). After adaptive training, the harmonic light can be focused on different spots for different input modes (Figure 6b). The intensity profile is utilized for classification as in the linear case. Those intensity profiles for all 15 modes are recorded to form the transfer matrix in Figure 6c. The SNR is 19.2 from the transfer matrix, which is slightly lower than the linear network in Figure 2. Due to the nonlinear interaction inside the nonlinear disordered sample, the output pattern of composed modes is not simply the superposition of singular modes. Therefore, the nonlinear network optimized for classification according to Equation (2) cannot be used directly for decomposition. Alternatively, the multiple modes are displayed in a time-sharing way and the output patterns are recorded only as a reference. When inputting multiple modes, bright spots also emerge at the corresponding positions (Figure 6d).

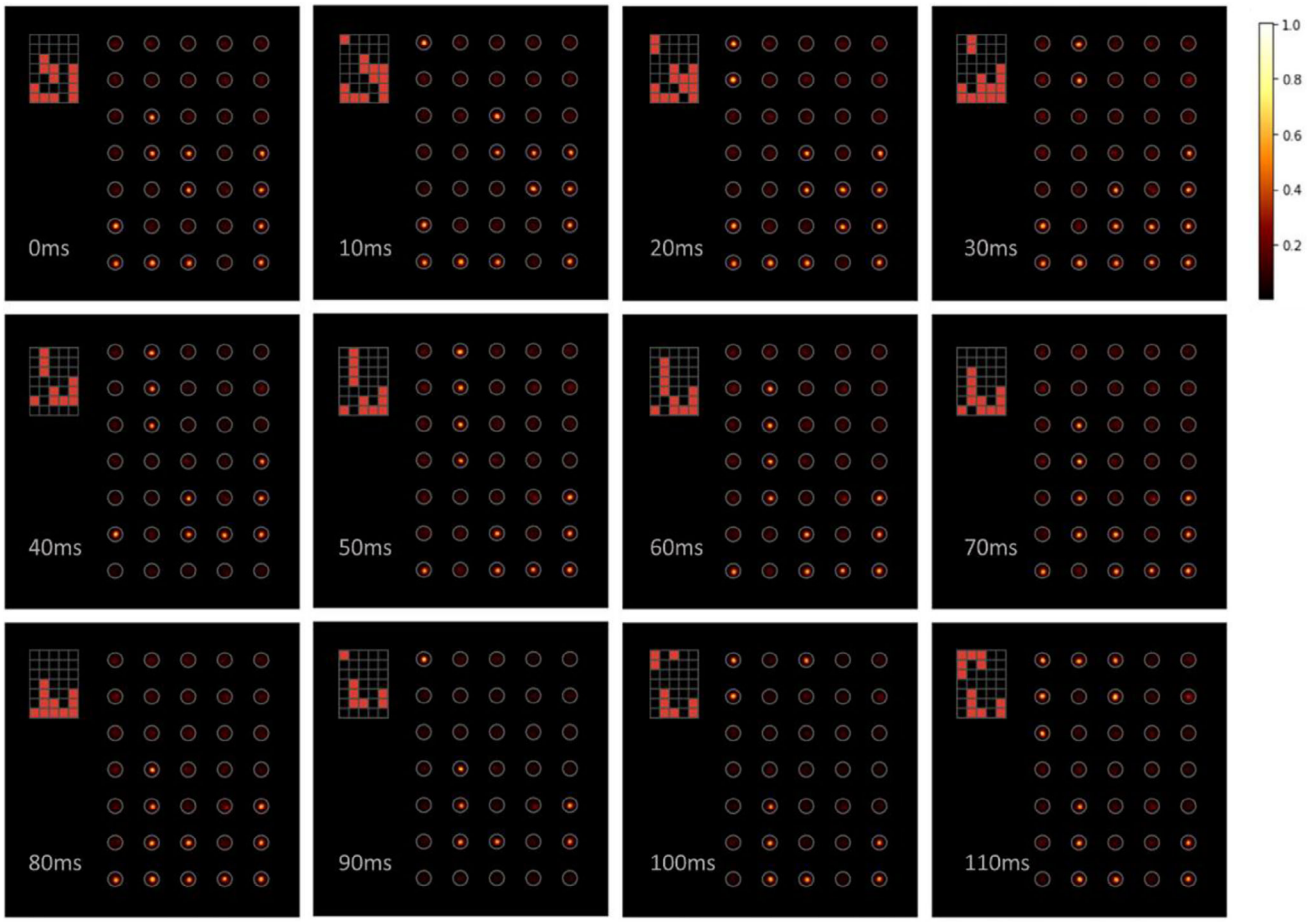

Figure 5. Live video transmission through a turbid medium: output image captured for subsequent frames of an input homemade comic (See the Video S1, Supporting Information).

Compared to the linear network, the nonlinear network is more difficult to train since the light source is a femtosecond pulsed laser (Figure S2, Supporting Information) which is hard to stay stable for a long time. Also, the complicated nonlinear interaction limits its utilization in modal decompositions and imaging. Therefore, we only demonstrate it in modal classification but not in more advanced tasks. However, those results still indicate that our platform based on a nonlinear disordered medium would be a good candidate for multi-layer nonlinear ONNs.

4. Conclusion

We demonstrated a multi-functional ONN based on the architecture of disordered medium and wavefront shaping. This architecture can realize both arbitrary linear operations within a specific size. For different linear operations, the network is modified only by switching the phase patterns on the SLM, while all the mechanical parts, lenses, and disordered samples are unchanged. Therefore, it can work as a universal ONN for various tasks including optical modal decomposition, image classification, and image transmission through diffusers. Compared with the digital methods, our setup directly operates on the light field and thus avoids the complicated wavefront measuring processes. Different from the diffraction neural networks with multiple SLMs, our method utilizes the disordered medium for connecting the modulated modes. Therefore, it needs only a single SLM to achieve comparable performances. Also, since the scattering inside the disordered medium has scrambled the spatial structure, the position of the sampling positions in the output plane can be arbitrarily assigned, which is not the case in diffraction neural networks[7] or Fourier neural networks[9] and might provide more freedom in imaging. Moreover, such a platform could also be trained to accelerate various time-consuming imaging tasks, such as super-resolution imaging[43,44] and wavefront measurement.[28] In our current setup, as a demonstration, the frame rates of the test input fields are still limited below 100 Hz due to the limitation of camera image acquisitions. However, this is not always an inherent limit since one can replace the camera with photodetectors placed at sampling positions. Also, the input field can be modulated with electro-optical modulators rather than DMD for high-speed purposes and the parallel field processing rate would be increased to gigahertz.

The major deficiency in the current work is a long time (several hours) for network training, especially for image classification which has a large dataset. To keep the disordered medium stable for such a long time, it also has a high requirement on

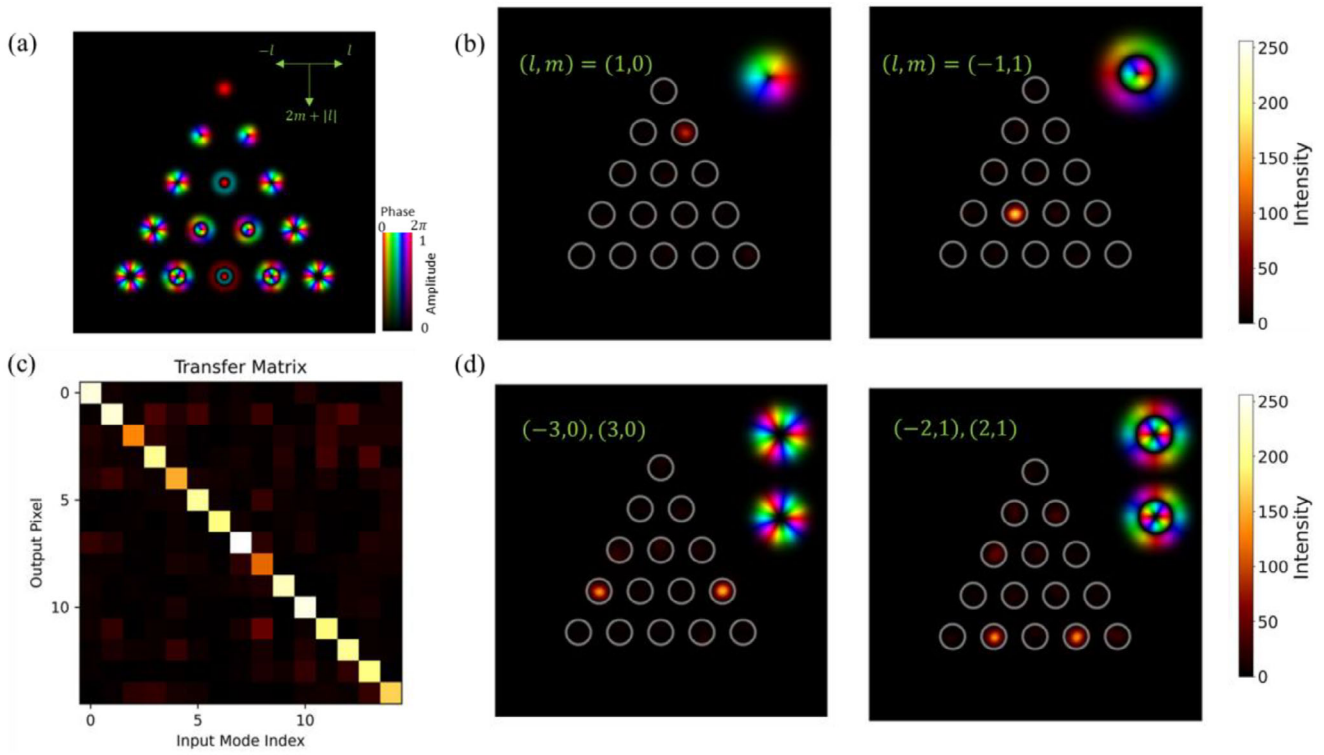

Figure 6. LG mode classification with nonlinear ONN. a) the field profile for all the 15 LG modes to be classified. b) Classification results for input modes (1,0) and (−1,1). c) Transfer matrix between input mode and output spot. d) Modal classification results when displaying multiple input fields in a time-sharing way.

mechanical components, external vibration, sample temperature, light sources' stability, and various aspects. The problem is more serious for nonlinear ONN where the applied pulsed laser source is hard to keep highly stable. Due to those issues, the nonlinear ONN is only demonstrated for a simple LG modal classification and has not manifested its power. To accelerate the training and address those problems, one needs to develop more advanced training algorithms, which deserve further investigations in the future.

Supporting Information

Supporting Information is available from the Wiley Online Library or from the author.

Acknowledgements

This work was supported by the National Science Foundation of China (Grant No. 12274295), Shanghai Technology Innovation Project (Grant No. 24590711300), and the National Key Research and Development Program (Grant Nos. 2023YFA1407200 and 2023YFB3906400).

Conflict of Interest

The authors declare no conflict of interest.

Data Availability Statement

The data that support the findings of this study are available from the corresponding author upon reasonable request.

Keywords

optical neural network, wavefront shaping

Received: June 6, 2025
Published online: July 5, 2025

[1] B. J. Shastri, A. N. Tait, T. Ferreira de Lima, W. H. P. Pernice, H. Bhaskaran, C. D. Wright, P. R. Prucnal, *Nat. Photonics* **2021**, *15*, 102.
[2] J. Liu, Q. Wu, X. Sui, Q. Chen, G. Gu, L. Wang, S. Li, *PhotoniX* **2021**, *2*, 5.
[3] X. Sui, Q. Wu, J. Liu, Q. Chen, G. Gu, *IEEE Access* **2020**, *8*, 70773.
[4] T. Zhou, X. Lin, J. Wu, Y. Chen, H. Xie, Y. Li, J. Fan, H. Wu, L. Fang, Q. Dai, *Nat. Photonics* **2021**, *15*, 367.
[5] Y. Chen, M. Nazhamaiti, H. Xu, Y. Meng, T. Zhou, G. Li, J. Fan, Q. Wei, J. Wu, F. Qiao, L. Fang, Q. Dai, *Nature* **2023**, *623*, 48.
[6] X. Luo, Y. Hu, X. Ou, X. Li, J. Lai, N. Liu, X. Cheng, A. Pan, H. Duan, *Light: Sci. Appl.* **2022**, *11*, 158.
[7] Y. Zuo, Y. Zhao, Y.-C. Chen, S. Du, J. Liu, *Phys. Rev. Appl.* **2021**, *15*, 054034.
[8] G. Ma, J. Yu, R. Zhu, C. Zhou, *Photonics Res.* **2023**, *11*, 299.
[9] X. Lin, Y. Rivenson, N. T. Yardimci, M. Veli, Y. Luo, M. Jarrahi, A. Ozcan, *Science* **2018**, *361*, 1004.

[10] Y. Luo, Y. Zhao, J. Li, E. Çetintaş, Y. Rivenson, M. Jarrahi, A. Ozcan, *eLight* **2022**, *2*, 4.
[11] J. Li, Y. Li, T. Gan, C. Shen, M. Jarrahi, A. Ozcan, *Light: Sci. Appl.* **2024**, *13*, 120.
[12] Y. Zhang, Q. Zhang, H. Yu, Y. Zhang, H. Luan, M. Gu, *Sci. Adv.* **2024**, *10*, adn2205.
[13] T. Wang, M. M. Sohoni, L. G. Wright, M. M. Stein, S.-Y. Ma, T. Onodera, M. G. Anderson, P. L. McMahon, *Nat. Photonics* **2023**, *17*, 408.
[14] Y. Zhou, B. Braverman, A. Fyffe, R. Zhang, J. Zhao, Alan E. Willner, Z. Shi, Robert W. Boyd, *Nat. Commun.* **2021**, *12*, 1866.
[15] K. Lu, Z. Chen, H. Chen, W. Zhou, Z. Zhang, H. K. Tsang, Y. Tong, *Nat. Commun.* **2024**, *15*, 3515.
[16] A. Jha, C. Huang, H. Peng, W. Zhang, B. Shastri, Paul R. Prucnal, "High-speed time series prediction and classification on an all-optical neural network", Optical Fiber Communication (OFC) Conference, San Diego, CA, USA, **2022**.
[17] M. Rafayelyan, J. Dong, Y. Tan, F. Krzakala, S. Gigan, *Phys. Rev. X* **2020**, *10*, 041037.
[18] Y. Shen, N. C. Harris, S. Skirlo, M. Prabhu, T. Baehr-Jones, M. Hochberg, X. Sun, S. Zhao, H. Larochelle, D. Englund, M. Soljačić, *Nat. Photonics* **2017**, *11*, 441.
[19] B. Zhao, J. Cheng, B. Wu, D. Gao, H. Zhou, J. Dong, *Opto-Electron. Sci.* **2023**, *2*, 230017.
[20] Y. Guo, S. Zhang, M. Pu, Q. He, J. Jin, M. Xu, Y. Zhang, P. Gao, X. Luo, *Light: Sci. Appl.* **2021**, *10*, 63.
[21] R. Fickler, M. Ginoya, R. W. Boyd, *Phys. Rev. B* **2017**, *95*, 161108(R).
[22] N. K. Fontaine, R. Ryf, H. Chen, D. T. Neilson, K. Kim, J. Carpenter, *Nat. Commun.* **2019**, *10*.
[23] S. Popoff, G. Lerosey, M. Fink, A. Claude Boccara, S. Gigan, *Nat. Commun.* **2010**, *1*, 81.
[24] C. He, D. Zhao, F. Fan, H. Zhou, X. Li, Y. Li, J. Li, F. Dong, Y.-X. Miao, Y. Wang, L. Huang, *Opto-Electron. Adv.* **2024**, *7*, 230005.
[25] Y. Liu, Y. Li, *Opto-Electron. Adv.* **2024**, *7*, 240057.
[26] E. Khoram, A. Chen, D. Liu, L. Ying, Q. Wang, M. Yuan, Z. Yu, *Photonics Res.* **2019**, *7*, 23.
[27] I. M. Vellekoop, A. P. Mosk, *Opt. Lett.* **2007**, *32*, 2309.
[28] S. M. Popoff, G. Lerosey, R. Carminati, M. Fink, A. C. Boccara, S. Gigan, *Phys. Rev. Lett.* **2010**, *104*, 100601.
[29] M. W. Matthès, P. del Hougne, J. de Rosny, G. Lerosey, S. M. Popoff, *Optica* **2019**, *6*, 465.
[30] A. Saade, F. Caltagirone, I. Carron, L. Daudet, A. Drémeau, S. Gigan, *2016 IEEE International Conference on Acoustics, Speech and Signal Processing (ICASSP)*, Shanghai, China, **2016**, 6215–6219.
[31] M. Baudrier-Raybaut, R. Haïdar, P. Kupecek, P. Lemasson, E. Rosencher, *Nature* **2004**, *432*, 374.
[32] F. Ni, H. Liu, Y. Zheng, X. Chen, *Adv. Photon.* **2023**, *5*, 046010.
[33] H. Wang, J. Hu, A. Morandi, A. Nardi, F. Xia, X. Li, R. Savo, Q. Liu, R. Grange, S. Gigan, *Nat. Comput. Sci.* **2024**, *4*, 429.
[34] J. Yang, Q. He, L. Liu, Y. Qu, R. Shao, B. Song, Y. Zhao, *Light: Sci. Appl.* **2021**, *10*, 149.
[35] Y. Zhao, Q. He, S. Li, J. Yang, *Opt. Lett.* **2021**, *46*, 1518.
[36] T. Wu, M. Guillon, G. Tessier, P. Berto, *Optica* **2024**, *11*, 297.
[37] S. A. Goorden, J. Bertolotti, A. P. Mosk, *Opt. Express* **2014**, *22*, 17999.
[38] H. Yan, Y. Sun, Y. Lin, F. Chu, W. Wan, *Opt. Express* **2023**, *31*, 22649.
[39] W. Liu, Z. Zhou, L. Chen, X. Luo, Y. Liu, X. Chen, W. Wan, *Opt. Express* **2021**, *29*, 29972.
[40] J. Bertolotti, E. G. van Putten, C. Blum, A. Lagendijk, W. L. Vos, A. P. Mosk, *Nature* **2012**, *491*, 232.
[41] J. Bertolotti, O. Katz, *Nat. Phys.* **2022**, *18*, 1008.
[42] T. Zhou, L. Fang, T. Yan, J. Wu, Y. Li, J. Fan, H. Wu, X. Lin, Q. Dai, *Photonics Res.* **2020**, *8*, 940.
[43] G. Zheng, R. Horstmeyer, C. Yang, *Nat. Photonics* **2013**, *7*, 739.
[44] Z. Zhou, W. Liu, J. He, L. Chen, X. Luo, D. Shen, J. Cao, Y. Dan, X. Chen, W. Wan, *Adv. Photon.* **2021**, *3*, 025001.